Site preference of S-doping and its influence on the properties of a Ni/Ni_3Al interface

2011 Modelling Simul. Mater. Sci. Eng. 19 065002

(http://iopscience.iop.org/0965-0393/19/6/065002)

Modelling Simul. Mater. Sci. Eng. **19** (2011) 065002 (16pp) doi:10.1088/0965-0393/19/6/065002

Site preference of S-doping and its influence on the properties of a Ni/Ni_3Al interface

L Peng[1,2], P Peng[1], D D Wen[1], Y G Liu[2], H Wei[3], X F Sun[3] and Z Q Hu[3]

[1] School of Materials Science and Engineering, Hunan University, Changsha 410082, People's Republic of China
[2] College of Environmental Science and Engineering, Hunan University, Changsha 410082, People's Republic of China
[3] Superalloy Division, Institution of Metal Research, CAS, Shenyang 110016, People's Republic of China

E-mail: ppeng@hnu.edu.cn

Received 15 March 2011, in final form 26 May 2011
Published 11 July 2011
Online at stacks.iop.org/MSMSE/19/065002

Abstract

A first-principles investigation of the doping effects of S on the properties of a Ni/Ni_3Al interface is conducted. S-doping is found to be energetically permissible either at sub-lattice sites or at octahedral interstitial centers, and S atoms prefer to substitute host atoms, especially Ni atoms, at the coherent $(0\,0\,2)\gamma/\gamma'$ layer. Among octahedral interstitial centers, the most favorable condition is the S segregation onto an octahedral interstice bounded by 6 Ni atoms at the coherent interfacial layer. The calculation of Griffith rupture work W and local bond overlap population shows that S-doping not only reduces the rupture strength of the Ni/Ni_3Al interface, especially at preferentially occupied sites, but also causes the inter-phase fracture mode and site to be changed. Doping with the trace element sulfur is indeed deleterious for the strengthening of the Ni/Ni_3Al interface; however, the segregation of S-doping onto the octahedral interstitial sites at the $(0\,0\,1)\gamma$ or the coherent $(0\,0\,2)\gamma/\gamma'$ layer is demonstrated to be profitable for improvement of the local toughness of the Ni/Ni_3Al interface to some extent, particularly in their inter-phase fracture regions. The S-induced embrittlement of the Ni/Ni_3Al interface can be attributed to a variation in atomic bonding energy. As S replaces Ni at the $(0\,0\,1)\gamma$ layer or located at the octahedral interstices at the $(0\,0\,1)\gamma$ layer or the coherent $(0\,0\,2)\gamma/\gamma'$ layer, the large local elastic strain energy in the inter-phase fracture regions should be responsible for the change in the inter-phase fracture sites.

(Some figures in this article are in colour only in the electronic version)

Introduction

Ni-based single crystal (SC) superalloys, which mainly consist of a high volume fraction of $\gamma\prime$ phase (a $L1_2$-type ordered Ni_3Al-based intermetallic compound) coherently dispersed on a γ matrix (a disordered fcc Ni-based solid solution with A_1 structure), are one of the key structural materials for high-temperature applications in advanced aero-engines and gas turbines. Their unique high-temperature mechanical properties largely originate from interactions of coherent $\gamma\prime$ precipitates with the γ-matrix, specially the $\gamma/\gamma\prime$ interface. In-service examination and failure analyses have shown that the structure and properties of the γ/γ' interface have a great influence on the shape, size and coarsening rate of γ' precipitates which in return strongly affect the creep strength or creep rupture life of SC superalloys subjected to stress at elevated temperatures [1].

Many experiments have demonstrated that trace elements and minor alloying additions, e.g. N, O, H, S, P, Si, As, Se, C, B, etc, have a great influence on the strength and ductility of Ni-based SC superalloys [2]. As is well known, sulfur is present in raw materials and at each step of alloy processing, strongly segregates on metal-free surfaces and at metal/oxide interfaces [3]. Previous experimental [4, 5] and theoretical [6] studies indicated that the segregation of S impurities at these interfaces has deleterious effects on the adherence of oxide scales. Therefore, sulfur is usually regarded as a detrimental non-metallic impurity in the majority of directionally solidified (DS) superalloys, because it not only causes the degradation of oxidation resistance by deteriorating the thermal barrier coating (TBC) adherence [3] but also reduces grain boundary ductility resulting in DS grain boundary cracking and weld solidification cracking [7]. However, unlike sulfur segregation at the surface of DS superalloys and its role on oxide layer adherence [5, 6], the occupation behavior of S at the γ-Ni/γ'-Ni_3Al interface and its effect on interfacial properties are scarcely reported in the literature. Hence an in-depth and thorough understanding of site preference of S-doping and its roles on strength and toughness of the γ/γ' interface is desired in order to guide the control of trace elements and minor alloying additions in Ni-based SC superalloys.

Since experimental techniques are still limited for detecting trace impurities at the γ-Ni/γ'-Ni_3Al interface, a sole option is the quantum-mechanism theoretical calculation based on density functional theory (DFT). In the past decade, several efforts have been made for understanding the adhesive properties of the γ-Ni/γ'-Ni_3Al interface in SC superalloys, especially strengthening and toughening effects of dopants [8–10] or additions [11–15]. Using a discrete variational X_α (DV-X_α) method, Liu *et al* [8] first investigated the doping effect of the Ni/Ni_3Al interface and found that the binding strength of the doped interfaces gradually decreased in the following order: C, B, N, O, H, clean, P, S. Later, Chen *et al* [9] further performed a first-principles calculation on the bonding characteristics of S-doped Ni/Ni_3Al interface by means of a molecular orbital DMol package. Their results indicated that a strong bonding between S and Ni atoms lying within the interface, which leads to an increase in the shear strength of the interface over the cohesive strength, is responsible for S-induced embrittlement of the Ni/Ni_3Al interface and this interfacial embrittlement can be relieved by substituting Al by Re at the Ni/Ni_3Al interface. By the first-principles plane-wave pseudo-potential method and CASTEP program, Peng *et al* [10] also investigated the effect of B and P on Griffith rupture work and local toughness of the Ni/Ni_3Al interface and revealed that B is beneficial to increase the interfacial fracture strength, while P has a deleterious effect. Recently, Wu *et al* [16] investigated the segregation behavior of B and H in Ni-based and Ni_3Al-based alloys by means of cluster models and a DV-X_α method. The results showed both B and H may segregate onto the octahedral interstices in the Ni/Ni_3Al interface but boron has a greater segregation tendency and higher stability than hydrogen. They pointed out that B-induced

ductility and H-induced embrittlement originate mainly from a different lattice misfit [17]. Very recently, Sanyal *et al* [18] further estimated effects of O, H and N on the cleavage energy of the Ni/Ni_3Al interface on the basis of an evaluation of their site preference with the help of *ab initio* VASP software. They found that O and H have intrinsic tendencies to segregate onto the octahedral interstice constituted by 6 Ni atoms in the interface. However, different from the embrittlement order suggested by Liu *et al* [8] in terms of the binding strength of cluster interfacial models, a careful calculation of Griffith rupture work in their interfacial supercell model showed that O has the most deleterious effect on interfacial embrittlement, followed by N and H. In fact, in our earlier investigation on the Re alloying effect [12], a supercell model was also demonstrated to be more suitable and reasonable than the corresponding cluster model for simulation and calculation of the electron interaction and cohesive property of the Ni/Ni_3Al interface. It is noted that previous investigation on S-induced embrittlement of the γ-Ni/γ'-Ni_3Al interface performed by Chen *et al* [9] seldom took into account the influence of the atoms far away from the Ni/Ni_3Al interface on the interfacial bonding strength. In addition, the site preference of S-doping in the Ni/Ni_3Al interfacial region was not considered in their cluster model. Therefore, in this paper, a series of Ni/Ni_3Al interfacial supercells S-doped at various sub-lattice sites and octahedral interstitial centers will be constructed and adopted to evaluate the doping effect on the cleavage energy and local toughness of the Ni/Ni_3Al interface. And particular attention will be paid to site preference of S-doping and geometrical structure change of the Ni/Ni_3Al interface induced by sulfur.

1. Method and model of computation

Cambridge Serial Total Energy Package (CASTEP), a first-principles plane-wave pseudo-potential method [19, 20] based on DFT, is employed to investigate the energetics and electronic structures of the Ni/Ni_3Al interface with S-doping. Ultrasoft pseudo-potentials [21] represented in reciprocal space with the GGA-PBE exchange-correlation function [22] were used for all elements in our models. In our calculations, the cutoff energy of atomic wave functions (PWs), E_{cut}, is set at 270 eV. A finite basis set correction [23] is applied for evaluation of energy and stress. In the calculation of self-consistent field (SCF), the Pulay scheme of density mixing [24] is adopted.

The same supercell model of the Ni/Ni_3Al interface as [10, 12] is built, as shown in figure 1, in which the (0 0 2) atomic layer is taken as a coherent interface of the γ-Ni and $\gamma\prime$-Ni_3Al phase based on the experimental result reported by Harada *et al* [25]. The lattice constant of the supercell is taken to be equal for γ-Ni and $\gamma\prime$-Ni_3Al blocks due to the assumption of complete coherence. The interaction between two adjacent interfaces is neglected [12]. Since the (0 0 2) atomic layer can be regarded as either the surface of the γ-Ni block or that of the $\gamma\prime$-Ni_3Al block, there exist two orientation relationships of $(0\,0\,2)\gamma \parallel (0\,0\,1)\gamma\prime$ and $(0\,0\,1)\gamma \parallel (0\,0\,2)\gamma\prime$ in the proposed interfacial model. Correspondingly, there are four constructional surface models, i.e. the (0 0 2) surface model of γ-Ni phase and the (0 0 1) surface model of $\gamma\prime$-Ni_3Al phase, and the (0 0 1) surface model of γ-Ni phase and the (0 0 2) surface model of $\gamma\prime$-Ni_3Al phase, respectively. In order to investigate the effect of S-doping on the strength and toughness of the Ni/Ni_3Al interface, four octahedral interstitial S-doped models, i.e. O-1, O-2, O-3 and O-4, and four substituted models by S-doping, i.e. Ni-1, Ni-2, Ni-3 and Al-4, are constructed. The sites occupied or replaced by S-doping in the above models are labeled in figure 1. For consideration of symmetry, the $\gamma/\gamma\prime$ interfacial supercell is doped by two S atoms, which are partitioned to two interfaces, and the symmetry of their distribution is maintained in our calculations.

All atomic positions in the supercell with and without S-doping are first relaxed according to the total energy and force using the BFGS scheme [26], based on the cell optimization

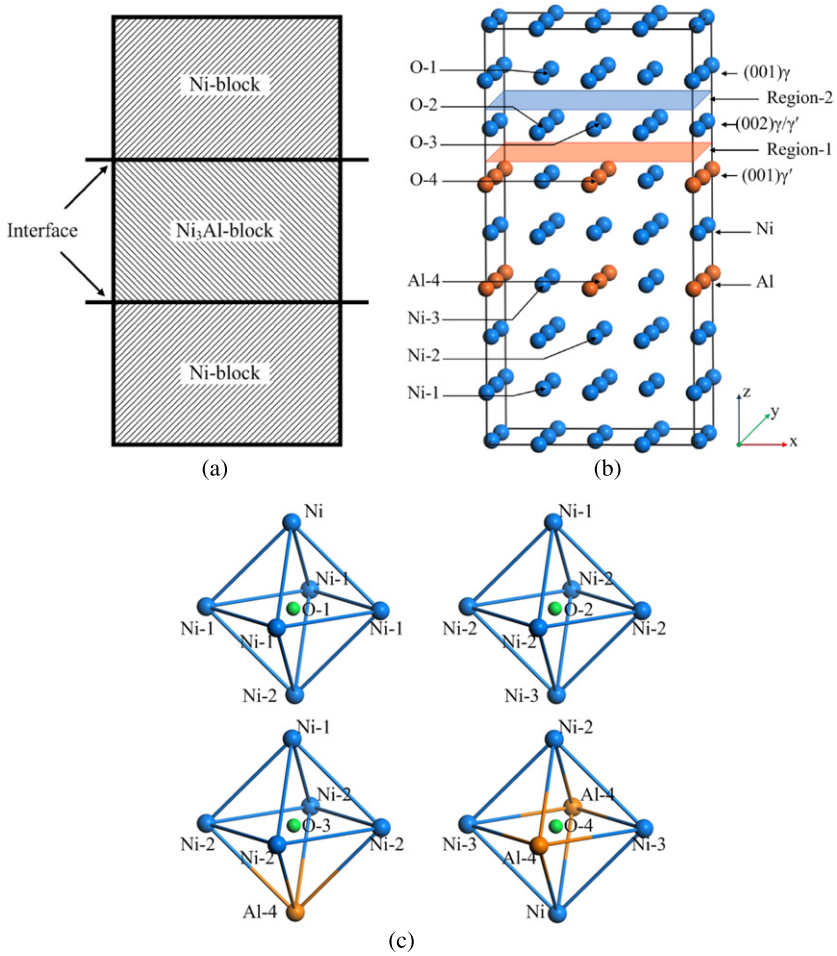

Figure 1. The γ-Ni/$\gamma\prime$-Ni$_3$Al interfacial model: (*a*) schematic diagram of the Ni/Ni$_3$Al interface; (*b*) the Ni/Ni$_3$Al supercell model; (*c*) several typical interstitial octahedrons in the Ni/Ni$_3$Al supercell. The blue, orange and green balls denote Ni, Al and S atoms, respectively. $(0\,0\,1)\gamma$, $(0\,0\,1)\gamma'$ and $(0\,0\,2)\gamma/\gamma'$ represent the $(0\,0\,1)$ atomic layer in the γ-Ni block, the $(0\,0\,1)$ atomic layer in the γ'-Ni$_3$Al block and the coherent Ni/Ni$_3$Al interfacial layer, respectively. Region-1 and region-2 are the region bounded by $(0\,0\,2)\gamma/\gamma'$ and $(0\,0\,1)\gamma'$ layers and by $(0\,0\,1)\gamma$ and $(0\,0\,2)\gamma/\gamma'$ layers, respectively. Ni-1, Ni-2, Ni-3, Al-4 and O-1, O-2, O-3, O-4 denote sub-lattice sites and octahedral interstitial centers in the Ni/Ni$_3$Al supercell, respectively.

criterion (RMS force of 0.05 eV Å^{-1}, RMS stress of 0.1 GPa and RMS displacement of 2.0×10^{-3} Å). The calculation of total energy and electronic structure is followed by cell optimization with a SCF tolerance of 2.0×10^{-5} eV /atom.

2. Results and discussion

2.1. Stress relaxation of the Ni/Ni$_3$Al interface caused by S-doping

After cell optimization, the displacement of host and doped atoms and the space between atomic layers in the Ni/Ni$_3$Al supercell are examined and tabulated in tables 1 and 2. From

Table 1. Relative displacement of doped and host atoms in the Z-direction. Note: positive and negative values represent the displacement toward and away from the coherent interfacial layer, respectively. The data in parentheses denote a relative displacement of host atoms adjacent to S-doping in the X- or Y-direction.

		Model							
Layer	Species	Ni-1	Ni-2	Ni-3	Al-4	O-1	O-2	O-3	O-4
(0 0 1)γ	Ni					(9.1%)	−23.2%	−34.9%	
	S	+31.9%				+13.8%			
(0 0 2)γ/γ'	Ni					−21.7%	(8.9%)	(7.1%)	−18.2%
	S		−4.7%				−15.1%	−32.9%	
(0 0 1)γ'	Ni								(11.9%)
	Al							−5.7%	(16.8%)
	S			−2.3%	+32.7%				+11.4%

Table 2. Space between atomic layers in Ni block, Ni_3Al block, region-1 and region-2 in the Ni/Ni_3Al interfacial model with or without S-doping (unit Å).

Model	Clean	Ni-1	Ni-2	Ni-3	Al-4	O-1	O-2	O-3	O-4
Ni block	1.82	1.80	1.77	1.74	1.81	1.84	1.79	1.92	1.75
Region-2	1.83	**1.86**	1.80	1.77	1.83	**1.89**	**1.87**	**1.97**	1.85
Region-1	**1.84**	1.84	**1.77**	**1.74**	**1.86**	1.85	1.86	1.91	**1.92**
Ni_3Al block	1.85	1.85	1.77	1.79	1.85	1.84	1.76	1.89	1.93

table 1, one can see that for the substitution of Ni or Al atoms by S in the Ni/Ni_3Al interfacial region, few host atoms are removed except for the substituted atoms. The substitution of Ni-2 at the coherent (0 0 2)γ/γ' atomic layer or Ni-3 at the (0 0 1)γ' atomic layer causes only a slight displacement of doped atoms across the interface, i.e. along the Z-direction, while if Ni at the (0 0 1)γ layer or Al at the (0 0 1)γ' layer is substituted by S, an obvious relative displacement of doped atoms can be observed in the Z-direction. The doped atoms are pulled out from their originally inhabited (0 0 1)γ and (0 0 1)γ' atomic layers in Ni-1 and Al-4 models, respectively, and then are pushed toward the coherent interfacial atomic layer. The former causes an obvious increase in the separation between the (0 0 1)γ layer and coherent (0 0 2)γ/γ' layer, i.e. region-2, and the latter leads to a slight enlargement in the space between the (0 0 2)γ/γ' layer and (0 0 1)γ' layer, i.e. region-1; refer to table 2.

In the interstitial S-doping case, an evident displacement can also be detected for some host atoms in addition to S-doping. All the Ni and Al atoms adjacent to S-doping are found to be pushed away from their sub-lattice sites. And the longitudinal displacement, i.e. in the Z-direction, of Ni or Al atom at the upper and lower vertexes of the occupied octahedron is more than the horizontal displacement, i.e. in the X- or Y-direction, of host atoms at the S-doped atomic layers (refer to figure 1(c)). However, it is noticed that only a part of Ni or Al atoms at the upper and lower vertexes of the occupied octahedron depart from their sub-lattice sites. For example, only a Ni-2 in the O-1 model and a Ni-1 in the O-2 model move 21.7% and 23.2% relative to other Ni atoms at the (0 0 2)γ/γ' and the (0 0 1)γ layers, respectively. In addition, a distinct displacement of doped atoms in the Z-direction is also observed in all interstitial models, and they are displaced toward the same direction as the above activated Ni or Al at the upper and lower vertexes of the occupied octahedron. This indicates that the deformation of the interstitial S-doped Ni/Ni_3Al interface is the displacement of the whole distorted octahedron to some extent. Similarly to the substitution of host atoms, S-doping at octahedral interstices also results in a change in the space between atomic layers,

Table 3. Heat of formation H and the cohesive energy E per atom as well as the solution energy δ per S-doping atom in the Ni/Ni_3Al interfacial model.

Model	H(eV)	E(eV)	δ (eV)
Clean	−0.2522	5.1274	
Ni-1	−0.3622	5.0793	
Ni-2	−0.3633	5.0804	
Ni-3	−0.3447	5.0618	
Al-4	−0.2896	5.0475	
O-1	−0.3441	5.0709	−3.2624
O-2	−0.3449	5.0717	−3.2898
O-3	−0.3224	5.0493	−2.5489
O-4	−0.2833	5.0102	−1.2580

especially for region-1 and region-2. However, different from the S-free system, table 2 shows that the separation in region-2 is obviously bigger than that in region-1 in O-1, O-2 and O-3 models, which means interstitial S-doping causes an extension in space between the $(0\,0\,1)\gamma$ and coherent $(0\,0\,2)\gamma/\gamma\prime$ layers. Undoubtedly, these displacements of the doped atoms and their adjacent host atoms as well as the variation of interfacial separations will result in a change in energetics and electronic structures of the Ni/Ni_3Al interface, and will then cause the rupture strength, inter-phase fracture mode and site to be changed as in B- or P-doped system [10].

2.2. Site preference of S in the Ni/Ni_3Al interfacial region

Although experiments showed that a trace amount of sulfur exists in most Ni-based SC superalloys, it is still not known whether there is S-doping at the Ni/Ni_3Al interface. In order to examine the probability of S-doping emerging at the Ni/Ni_3Al interface and to further determine its site preference in the interfacial region, herein the heat of formation H and cohesive energy E of the Ni/Ni_3Al interfacial supercell are calculated by the following expressions [27]:

$$H = [E_i(n, m, l) - n \cdot E(\mathrm{Ni}) - m \cdot E(\mathrm{Al}) - l \cdot E(\mathrm{S})]/(m + n + l) \quad (1)$$

$$E = -[E_i(m.n.l) - n \cdot E_{\mathrm{Ni}} - m \cdot E_{\mathrm{Al}} - l \cdot E_{\mathrm{S}}]/(m + n + l) \quad (2)$$

where E_i (n, m, l) is the total energy of the γ-Ni/$\gamma\prime$-Ni_3Al interfacial supercell with n, m and l atoms of Ni, Al and S, respectively. E(Ni), E(Al) and E(S) are the energies per atom in the fcc-Ni, fcc-Al and orthorhombic S unit cells, respectively. E_{Ni}, E_{Al} and E_{S} are the energies per gaseous Ni, Al and S atoms, respectively. Table 3 lists the magnitude of $H$and E of the Ni/Ni_3Al interfaces with or without S-doping. A negative H in table 3 indicates S-doping at the Ni/Ni_3Al interface is permissible in terms of energetics [12]. The larger the negative heat of formation, the higher the formation ability of the doped $\gamma/\gamma\prime$ interface. In addition, the bigger the cohesive energy, the more stable the doped system [27]. Hence the following formation tendency of the Ni/Ni_3Al interface with or without S-doping can be deduced from the data presented in table 3: Ni-2 > Ni-1 > O-2 > Ni-3 > O-1 > O-3 > Al-4 > O-4 > clean, in which the clean model represents the Ni/Ni_3Al interface free of S. A larger negative H of the S-doped γ-Ni/$\gamma\prime$-Ni_3Al interface than that of the S-free system suggests that S can be doped in the Ni/Ni_3Al interfacial region by occupying octahedral interstitial sites or replacing a part of host atoms, similarly to B and H [17] as well as O and N [18]. In comparison with the interstitial sites, S prefers to substitute the host atoms, especially Ni atoms at the coherent $(0\,0\,2)\gamma/\gamma\prime$ layer. For interstitial S-doping at the coherent $(0\,0\,2)\gamma/\gamma\prime$ layer, the favorable site

is the O-2 octahedral interstitial center bounded by 6 Ni atoms rather than the O-3 octahedral interstice consisting of 5 Ni and a Al atoms as proposed in [9]. It is noted that all S-doped Ni/Ni_3Al systems are not as stable as the clean Ni/Ni_3Al interface. The stability of the Ni/Ni_3Al interfaces with or without S-doping decreases in the following order: clean > Ni-2 > Ni-1 > O-2 > O-1 > Ni-3 > O-3 > Al-4 > O-4. This means the Ni/Ni_3Al interface with S doped at the coherent $(0\,0\,2)\gamma/\gamma\prime$ layer has simultaneously high formation ability and structural stability.

Further, the tendency of S-doping segregation onto various interstitial sites of the Ni/Ni_3Al interface is determined by means of a comparison of the solid solution energy δ per doped atom. The solid solution energy δ is defined as a difference in the systemic binding energy ΔE between S-doped and S-free interfaces [18], i.e.

$$\delta = (\Delta E_{\text{doping}} - \Delta E_{\text{clean}})/l = [E_{\text{i}}(m, n, l) - E_i(m, n) - l \cdot E_{\text{S}}]/l. \tag{3}$$

The calculated δ are also tabulated in table 3. Similarly to the variation tendency of the heat of formation H and the cohesive energy E, table 3 shows that δ in the O-2 model is also the biggest among the four interstitial models, followed by O-1, O-3 and O-4 models in turn. As is well known, the bigger the δ, the stronger the segregation tendency of doping onto heterogeneous interfaces and grain boundaries [6, 18], hence S will prefer to segregate onto the octahedral interstitial site bounded by 6 Ni atoms at the coherent $(0\,0\,2)\gamma/\gamma\prime$ interfacial layer, then O-1 site at the $(0\,0\,1)\gamma$ layer, followed by O-3 site bounded by 5 Ni and 1 Al atoms at the $(0\,0\,2)\gamma/\gamma\prime$ layer, and finally O-4 site at the $(0\,0\,1)\gamma\prime$ layer. Thus, the following investigation on the strength of the Ni/Ni_3Al interface with S-doping will mainly focus on the case of S segregation onto the octahedral interstitial sites at the coherent $(0\,0\,2)\gamma/\gamma\prime$ layer.

2.3. Griffith rupture work of doped Ni/Ni_3Al interfaces

As is well known, the γ-Ni/$\gamma\prime$-Ni_3Al interface is the weakest site in Ni-based SC superalloys. The binding strength of the $\gamma/\gamma\prime$ interface can be regarded as a representative of the rupture strength of SC superalloys to some extent [12]. Herein a work of separation, i.e. Griffith rupture work W [28], which is defined as the reversible work needed to separate a crystal along the interface into two free surfaces, is employed to evaluate the binding strength of the Ni/Ni_3Al interface. Wcan be calculated by means of the difference in total energy between the interfacial model and the corresponding surface models:

$$W = (-1/2S_{\text{i}}) \cdot [E_{\text{i}}(n, m, l) - E_{\text{S}}^{\gamma}(n_\gamma, m_\gamma, l_\gamma) - E_{\text{S}}^{\gamma'}(n_{\gamma'}, m_{\gamma'}, l_{\gamma'})] \tag{4}$$

where S_{i} is an area of coherent atomic layer in the Ni/Ni_3Al interfacial model. $E_{\text{S}}^{\gamma}(n_\gamma, m_\gamma, l_\gamma)$ and $E_{\text{S}}^{\gamma'}(n_{\gamma'}, m_{\gamma'}, l_{\gamma'})$ are the total energies of unrelaxed surface models of the γ-Ni and $\gamma\prime$-Ni_3Al blocks, respectively, corresponding to the Ni/Ni_3Al interfacial model. n, m, ldenote the numbers of Ni, Al and S atoms, respectively, where $n = n_\gamma + n_{\gamma\prime}$, $m = m_\gamma + m_{\gamma\prime}$, $l = l_\gamma + l_{\gamma\prime}$. Herein, the surface models truncated from the optimized interfacial supercells will not be relaxed in the calculation of the cleavage work W.

Table 4 tabulates the total energies of the Ni/Ni_3Al interfacial and correlated surface models as well as the Griffith rupture work calculated using equation (4). Considering the existence of two orientation relationships in the present Ni/Ni_3Al interfacial model, i.e. $(0\,0\,2)\gamma \parallel (0\,0\,1)\gamma\prime$ and $(0\,0\,1)\gamma \parallel (0\,0\,2)\gamma\prime$, there are two potential inter-phase fracture sites [10], i.e. region-1 and region-2. In the first mode the cleavage adjacent to the coherent $(0\,0\,2)$ layer occurs along the $(0\,0\,1)\gamma'$ layer in the γ'-Ni_3Al block, while in the second one the split occurs along the $(0\,0\,1)\gamma$ layer in the γ-Ni block. From table 4, one can see that in the case of the clean interfacial model Win region-1 is smaller than that in region-2. Usually, fracture occurs at the weakest part of a material [28]. Therefore the Griffith rupture work$W$ in region-1, 4.298 J m^{-2}, represents the

Table 4. Total energies of Ni/Ni_3Al interfacial supercells (E_i) and the corresponding surface models (E_S), the interfacial areas (S_i) as well as the Griffith rupture works (W) in different interfacial regions.

Model	Site	E_i (eV)	E_S^{γ} (eV)	$E_S^{\gamma'}$ (eV)	S_i (Å^2)	W(J m^{-2})
Clean	Region-1	−76 422.43	−54 235.12	−22 160.30	50.32	**4.298**
	Region-2	−76 422.43	−32 535.48	−43 859.31		4.399
Ni-1	Region-1	−74 267.32	−52 080.12	−22 159.45	51.83	4.288
	Region-2	−74 267.32	−30 382.46	−43 858.09		**4.138**
Ni-2	Region-1	−74 267.39	−52 084.01	−22 160.25	50.32	**3.680**
	Region-2	−74 267.39	−32 535.64	−41 708.08		3.766
Ni-3	Region-1	−74 266.20	−54 232.63	−20 004.96	54.32	**4.219**
	Region-2	−74 266.20	−32 533.94	−41 702.90		4.330
Al-4	Region-1	−76 861.17	−54 233.53	−22 600.10	51.91	**4.250**
	Region-2	−76 861.17	−32 534.77	−44 298.72		4.271
O-1	Region-1	−76 979.35	−54 791.50	−22 159.28	52.75	4.338
	Region-2	−76 979.35	−33 097.64	−43 857.79		**3.633**
O-2	Region-1	−76 979.41	−54 795.19	−22 159.13	53.22	3.777
	Region-2	−76 979.41	−32 534.12	−44 421.04		**3.650**
O-3	Region-1	−76 977.93	−54 794.224	−22 159.52	52.06	3.722
	Region-2	−76 977.93	−32 533.95	−44 421.55		**3.451**
O-4	Region-1	−76 975.34	−54 232.57	−22 718.75	53.82	**3.575**
	Region-2	−76 975.34	−32 534.34	−44 412.35		4.264

rupture strength of the clean interface [12]. In the case of S-doping, a similar evaluation is made. Table 4 indicates that both W in region-1 and in region-2 at the doped Ni/Ni_3Al interfaces are smaller than the rupture strength of the S-free interface. And the cleavage energy of the Ni/Ni_3Al interface with substitution of S for host atoms is generally larger than that of the interstitial S-doped Ni/Ni_3Al interface. For substituted Ni/Ni_3Al interfaces with stronger site preference of S-doping, table 4 shows that most of the W values in region-1 are smaller than those in region-2, e.g. in Ni-2 and Ni-3 models, which means the fracture site in these models is still region-1, as in the S-free interface, whereas in most of interstitial S-doped Ni/Ni_3Al interfaces with higher segregation ability, e.g. O-1 and O-2 models, the binding strength in region-1 is bigger than that in region-2, hence their inter-phase fracture site will be changed. A potential fracture site in these interstitial S-doped interfaces should be region-2 rather than region-1 as speculated previously [9]. In comparison with the clean Ni/Ni_3Al interface, the rupture strengths of the S-doped Ni/Ni_3Al interfaces decrease no matter cleavage fracture emerges in region-1 than does in region-2. The order of the rupture strength is as follows: clean > Al-4 > Ni-3 > Ni-1 > Ni-2 > O-2 > O-1 > O-4 > O-3. On the whole, S-doping has a deleterious effect on the rupture strength of the Ni/Ni_3Al interface, although the rupture strengths in Ni-1, Ni-3 and Al-4 models are close to that of the clean Ni/Ni_3Al interface. And an evident decrease in the rupture strength in Ni-2 and interstitial S-doped models can be seen. Relative to the S-free interface, the rupture strength of S-doped systems decreases by 14.4%, 15.1% and 19.7%, respectively, as a Ni sub-lattice site or O-2 and O-3 interstitial sites at the coherent (0 0 2)$\gamma/\gamma\prime$ layer is occupied by S. Since S prefers to substitute for Ni and to segregate onto the octahedral interstitial sites at the coherent (0 0 2)$\gamma/\gamma\prime$ interfacial layer, doping by the trace element sulfur is indeed deleterious for the strengthening of Ni-based SC superalloys [7].

2.4. Local toughness of Ni/Ni_3Al interfaces

In order to qualitatively evaluate the effect of S-doping on the local toughness of the Ni/Ni_3Al interface, the ionic and covalent bonding between first nearest neighbor (FNN) atoms of

Table 5. Mulliken's charge $Q(A)$ (unit: e) of atom A in the Ni/Ni_3Al interfacial supercell with or without S-doping. Note that the data in parentheses denote Q(S) at substituted sites.

Model	Q(S)	Q(Ni-1)	Q(Ni-2)	Q(Ni-3)	Q(Al-4)
Clean		0.01	−0.02	−0.08	0.19
Ni-1		(0.09)	−0.06	−0.05	0.19
Ni-2		0.00	(0.05)	−0.08	0.20
Ni-3		0.01	−0.04	(0.01)	0.20
Al-4		0.01	−0.06	−0.05	(0.12)
O-1	0.10	−0.07	−0.16	−0.05	0.19
O-2	0.15	−0.11	−0.07	−0.06	0.22
O-3	0.13	−0.12	−0.09	−0.06	0.25
O-4	−0.10	−0.01	−0.05	−0.11	0.24

the Ni/Ni_3Al interface are calculated using the Mulliken's population analysis method [29]. Mulliken's charge $Q(A)$ of A atom and bond overlap population Q_{A-B} between A and B atoms are defined as follows:

$$Q(A) = \sum_k w_k \sum_\mu^A \sum_\nu^A P_{\mu\nu}(k) S_{\nu\mu}(k) \tag{5}$$

$$Q_{A-B} = \sum_k w_k \sum_\mu^A \sum_\nu^B 2P_{\mu\nu}(k) S_{\mu\nu}(k) \tag{6}$$

where P_{uv} and S_{vu} are the density matrix and the overlap matrix, respectively, w_k is the weight associated with the calculated k-points in the Brillouin zone. Usually, the magnitude and sign of $Q(A)$ characterize the ionicity of A atom in a supercell; Q_{A-B} can be used to approximately measure the covalent bonding strength.

Table 5 lists the $Q(A)$ of Aatom in the Ni/Ni_3Al interfacial supercell. Herein, a small magnitude of Q(Ni) at Ni-1 and Ni-2 sites in the clean Ni/Ni_3Al model denotes the ionic bonding between FNN Ni–Ni in the γ-Ni block to be weak, while a notable charge transfer from Al at the $(0\,0\,1)\gamma\prime$ layer to Ni at the $(0\,0\,1)\gamma\prime$ and $(0\,0\,2)\gamma/\gamma\prime$ layers means a strong ionic bonding exists between FNN Ni–Al atoms, which is in agreement with that reported in [14]. For the S-doped interface, an evident charge transfer from S to Ni can also be observed, and this charge transfer is found to be correlated with the location and number of its FNN Al atoms. For example, the charge transfer of S at O-2 site is the most among S-doped systems. In the Ni-3 model, 4 Al atoms near by the doped atom significantly limit the number of electrons lost by S, while in the O-4 model, 2 Al close to the doped atom even make S obtain some electrons from its FNN Al atoms.

Considering the correlation between the brittleness or toughness of materials and the directionality of covalent bonds, in this section particular attention is paid to bond overlap population Q_{A-B} between FNN atoms in the Ni/Ni_3Al interfacial region. Table 6 lists Q_{A-B} between doped and host atoms as well as between host atoms in the Ni/Ni_3Al interface with or without S-doping. From table 6, one can see that $Q_{\text{Ni–Al}}$ is generally larger than $Q_{\text{Ni–Ni}}$ in the S-free model. And $Q_{A\text{-}B}$ between Ni at the $(0\,0\,2)\gamma/\gamma\prime$ layer and its FNN Ni exhibits a notable directionality, in which $Q_{\text{Ni-Ni}}$ between the $(0\,0\,1)\gamma$ and $(0\,0\,2)\gamma/\gamma\prime$ layers is distinctly larger than those within the $(0\,0\,2)\gamma/\gamma\prime$ layer and between the $(0\,0\,2)\gamma/\gamma\prime$ and $(0\,0\,1)\gamma\prime$ layers [14]. However, in the γ-Ni block, $Q_{\text{Ni-Ni}}$ is of a larger magnitude and shows an excellent isotropic build-up within a layer and between layers [9, 12]. Undoubtedly, the decrease in magnitude and the increase in directionality of $Q_{\text{Ni-Ni}}$ along and across the $(0\,0\,2)\gamma/\gamma\prime$ interfacial layer are

Table 6. Bond overlap populations (Q_{A-B}) between FNN atoms in the Ni/Ni_3Al interfacial supercells with or without S-doping.

Site		Q_{A-B}	Clean	Ni-1	Ni-2	Ni-3	Al-4	O-1	O-2	O-3	O-4
Intra-layer	(0 0 1)γ	Ni–Ni	0.11–0.12	0.11–0.13	0.03–0.09	0.10–0.11	0.11–0.12	0.00–0.14	0.11–0.12	0.08–0.14	0.09–0.12
		S–Ni		0.07				0.25–0.27			
	(0 0 2)γ/γ'	Ni–Ni	0.06	0.00–0.06	0 .03–0.05	0.03–0.05	0.00–0.05	0.06–0.08	0.00–0.08	0.00–0.07	0.07–0.13
		S–Ni			0.10				0.29	0.33	
	(0 0 1)γ'	Ni–Al	0.22	0.21–0.23	0.17–0.20	0.19–0.24	0.21–0.23	0.15–0.22	0.17–0.23	0.23–0.24	0.25–0.27
		S–Ni					0.08				0.31
		S–Al				0.01					0.30
Inter-layer	Region-1	Ni–Ni	0.04	0.01–0.06	0.00	0.02–0.06	0.00–0.04	0.02–0.05	0.00–0.09	0.05–0.07	0.00–0.07
		Ni–Al	0.19	0.19	0.15–0.20	0.18–0.21	0.18–0.22	0.19–0.29	0.17–0.20	0.06–0.25	0.15–0.22
		S–Ni			0.11	0.12	0.31		0.22		0.35
		S–Al			0.10					0.01	
	Region-2	Ni–Ni	0.10–0.13	0.05–0.12	0.08–0.12	0.09–0.13	0.09–0.14	0.08–0.14	0.09–0.15	0.08–0.12	0.09–0.15
		S–Ni		0.30	0.10			0.33	0.30	0.40	

caused mainly by the closeness to Al at the (0 0 1)$\gamma\prime$ layer which transfers part of its p electrons to the d shell of Ni-2 [30] (refer to table 5).

With the substitution of host atoms by S, the magnitude and directionality of Q_{A-B} in the Ni/Ni_3Al interfacial region varies distinctly, especially for Q_{A-B} between S-dopants and its FNN host atoms as well as between host atoms near the S-dopants. For example, the displacement of doped atoms toward the interface in the Ni-1 model not only leads to $Q_{S-Ni} = 0.30$ in region-2 to be obviously bigger than $Q_{S-Ni} = 0.07$ at the doped (0 0 1)γ layer, but also makes Q_{Ni-Ni} between Ni-2 and Ni-2 atoms near the S-dopants at the (0 0 2)$\gamma/\gamma\prime$ layer disappear. A similar variation can also be observed in the Al-4 model. Obviously, this evident difference in Q_{A-B} should be attributed to the displacement of doped atoms and the variation of layer spaces caused by S-doping (refer to tables 1 and 2). However, in Ni-2 and Ni-3 models, only a slight change takes place for Q_{A-B} between FNN host atoms, and their Q_{S-Ni} values within a layer are almost equal to those between layers. For these slightly deformed systems with S-doping, the following variation tendency of Q_{A-B} can be seen: $Q_{S-Ni} \approx Q_{Ni-Ni}$ but $Q_{S-Al} < Q_{Ni-Al}$. This weakening effect of S-doping on the directionality of covalent bonds between Ni–Al seems to imply that the substitution of Ni by S is advantageous in reducing the brittleness of the clean Ni/Ni_3Al interface to a certain extent.

For S-doping at interstitial sites in the Ni/Ni_3Al interface, figure 1(*c*) shows that six new strong covalent bonds between doped and host atoms will emerge in the occupied octahedrons, in which four Q_{A-B} locate at the doped atomic layer and other two Q_{A-B} situate in the region between adjacent atomic layers. From table 6 one can see that either for Q_{S-Ni} or for Q_{S-Al} their magnitude is different in various interstitial models and the bonding strength within a layer is generally smaller than that between layers. As a result of the synchronous displacement of S together with Ni-1 at a vertex of the occupied octahedron along the interface, Q_{S-Ni} in region-2 is only slightly larger than that in region-1 in the O-2 model, while a relative longitudinal displacement of S against Ni-1 and Al-4 at vertexes of the occupied octahedron leads to $Q_{S-Al} = 0.01$ in region-1 to be far smaller than $Q_{S-Ni} = 0.40$ in region-2 in the O-3 model. It is also noted that the distortion and the displacement of the whole interstitial octahedron induced by S-doping simultaneously cause a decrease in Q_{A-B} between host atoms at the vertexes of the doped octahedron in addition to the introduction of the above-mentioned six new covalent bonds. For example, four Q_{Al-Ni} in region-1 change to 0.06 from about 0.20 of the S-free system, meanwhile four Q_{Ni-Ni} within the (0 0 2)$\gamma/\gamma\prime$ layer vanish in the O-3 model.

Table 7. Intra-layer and inter-layer LBOP as well as their ratio (R_{LBOP}) in different interfacial regions in the Ni/Ni_3Al interfacial model.

	Model	Clean	Ni-1	Ni-2	Ni-3	Al-4	O-1	O-2	O-3	O-4
Intra-layer	$\mathrm{LBOP}_{(0\,0\,1)\gamma'}$	3.52	3.60	3.08	2.72	3.00	3.24	3.36	3.76	4.42
	$\mathrm{LBOP}_{(0\,0\,2)\gamma'/\gamma}$	0.96	0.56	0.88	0.68	0.60	1.08	2.04	2.16	1.52
	$\mathrm{LBOP}_{(0\,0\,1)\gamma}$	1.80	1.76	1.16	1.72	1.88	2.60	1.84	1.92	1.76
Inter-layer	$\mathrm{LBOP}_{(0\,0\,2)\gamma'/\gamma-(0\,0\,1)\gamma'}$	3.68	3.64	3.02	4.04	3.88	3.88	3.70	3.49	3.47
	$\mathrm{LBOP}_{(0\,0\,1)\gamma-(0\,0\,2)\gamma'/\gamma}$	3.68	3.84	2.84	3.40	3.44	3.47	3.58	3.28	3.90
Region-1	R_{LBOP}	**1.22**	1.14	**1.31**	**0.84**	**0.93**	1.11	1.46	1.70	**1.71**
Region-2	R_{LBOP}	0.75	**0.60**	0.72	0.71	0.72	**1.06**	**1.08**	**1.24**	0.84

This disorder variation of Q_{A-B} in the S-doped system indicates that the investigation on the S-induced embrittlement of the γ-Ni/γ'-Ni_3Al interface should take into account the mutual influence of doping and its local structural environment.

Similarly to the previous investigations on the effects of B, P [10] and Re [12] on the properties of the Ni/Ni_3Al interface, herein a local bond overlap population (LBOP) [17] is calculated and adopted to evaluate the bonding strengths within a layer and between layers. Intra-layer and inter-layer LBOP values are defined as the sum of bond overlap population along and across the Ni/Ni_3Al interface, respectively. And the ratio of the intra-layer LBOP to inter-layer LBOP [15], i.e. $R_{\mathrm{LBOP}} = \mathrm{LBOP}_{\text{intra-layer}}/\mathrm{LBOP}_{\text{inter-layer}}$, is further used to judge the competition of the ductile and brittle fracture modes of the Ni/Ni_3Al interface, as shown in table 7. Usually, a material would fail in a brittle manner if the ideal cohesive strength were reached along the extension of the crack before the ideal shear strength is reached [31]; hence a material would fail in brittle fracture mode if $R_{\mathrm{LBOP}} > 1$, in contrast, it would cleave in ductile fracture mode if $R_{\mathrm{LBOP}} < 1$ [9]. In addition, R_{LBOP} is also an excellent indicator of the directionality of the local covalent bonding in the Ni/Ni_3Al interfacial region. If the ratio of the number of covalent bonds in two intra-layers to that in the interlayer is R_0, then the closer the value of R_{LBOP} is to R_0, the better the local toughness is [12].

With reference to the S-free Ni/Ni_3Al interface, figure 1(*b*) shows the total number of covalent bonds within the $(0\,0\,1)\gamma$ and $(0\,0\,2)\gamma/\gamma'$ layers is equal to that between the $(0\,0\,1)\gamma$ and $(0\,0\,2)\gamma/\gamma'$ layers in region-2, and so is in region-1. Hence the R_0 value is $32/32 = 1$. In the case of S-doping, the substitution of host atoms by S does not change the intra-layer or inter-layer number of covalent bonds, whereas interstitial doping of S at octahedrons will lead to the number of covalent bonds within the doped layer and between the doped layer and its adjacent layer to be increased by 4 and 1, respectively, therefore the R_0 value in the interstitial S-doped systems will change to $(32+4)/(32+1) = 1.09$ except for region-1 in the O-1 model and region-2 in the O-4 model, in which the R_0 value is still 1 as in the clean and substituted interfaces.

For the clean interface, table 7 shows that both R_{LBOP} values in region-1 and in region-2 are close to 1, the deviations of R_{LBOP} from $R_0 = 1$ are 22% in region-1 and 25% in region-2, respectively, which means their interfacial regions are ductile to some extent [12, 16], but a bigger R_{LBOP} than 1 in region-1, i.e. the inter-phase fracture site (refer to table 4), indicates that the S-free Ni/Ni_3Al interface will fail in brittle fracture mode.

With respect to the S-doped Ni/Ni_3Al interface, the substitution of Ni atoms by S at the $(0\,0\,1)\gamma$ layer in the γ-block or at the coherent $(0\,0\,2)\gamma/\gamma'$ layer causes a significant variation in the magnitude of R_{LBOP}, especially in the inter-phase fracture site, e.g. region-2 in the Ni-1 model and region-1 in the Ni-2 model. A larger deviation of R_{LBOP} from 1 means their local toughness in these fracture regions is very low relative to the S-free interface. However,

different from Ni-1 and Ni-2 models, the R_{LBOP} values at the inter-phase fracture sites, i.e. region-1 in Ni-3 and Al-4 models, are close to and smaller than 1, which seems to imply the substitution of Ni or Al atom by S at the $(0\,0\,1)\gamma\prime$ layer in the $\gamma\prime$-block would be profitable to increase the local toughness of S-doped interfaces and their failure mode would be cleavage via shear, i.e. ductile fracture. Unfortunately, table 3 indicates that these substitutions are almost prohibited by their low formation ability and structural stability.

In the case of interstitial S-doping, table 7 shows that the R_{LBOP} in S-doped systems evidently increases, especially in region-1 in O-2, O-3 and O-4 models. A large increment in R_{LBOP} in region-1 seems to indicate that the interstitial S-doping would further degrade the local toughness of the clean Ni/Ni_3Al interface. However, it is noted that the R_{LBOP} values in region-2, i.e. the inter-phase fracture site, in O-1 and O-2 models are very close to their R_0, far superior to Ni-3 and Al-4 models. For example, the deviations of R_{LBOP} from R_0 in region-2 in O-1 and O-2 models are only 2.8% and 0.9%, respectively. Although the cleavage in O-1 and O-2 models still takes place in brittle fracture mode, their local brittleness at the inter-phase fracture sites is partially relieved. Hence, the segregation of S onto the octahedral interstitial sites at the $(0\,0\,1)\gamma$ layer or the coherent $(0\,0\,2)\gamma/\gamma\prime$ layer should be helpful for the improvement of the local toughness of the clean Ni/Ni_3Al interface to a certain extent. And among all the sites S-doping at the O-1 site is the most favorable, because the deviation of R_{LBOP} from R_0 either in region-1 or in region-2 is smaller than that in the clean interface. For the O-4 model, the $R_{\mathrm{LBOP}} = 1.71$ at the inter-phase fracture site, i.e. region-1, is far bigger than its $R_0 = 1.09$, which means this doped interface is of the lowest local toughness among the interstitial S-doped interfaces and fails in brittle fracture mode. Fortunately, this deleterious influence of S-doping may not be considered owing to its low formation ability and segregation tendency.

It is worth pointing out that then above toughening effect of S-doping at the coherent $(0\,0\,2)\gamma/\gamma\prime$ layer seems to be inconsistent with the embrittlement influence reported previously [9]. For S-doping at the O-3 octahedral interstitial site bounded by 5 Ni atoms and an Al atom, Chen *et al* [9] calculated the R_{LBOP} (in the Mayer form) in region-1 by the DMol molecular orbital package and found it to increase by 121% compared with the S-free interface; thereby they concluded S-doping should deteriorate the embrittlement degree of the clean interface. However, as elucidated in section 2.2, the present calculation for Griffith fracture work W indicates that the Ni/Ni_3Al interface with S doped at the O-3 interstitial site would be cleaved along the $(0\,0\,1)\gamma$ layer in region-2 rather than along the $(0\,0\,1)\gamma\prime$ layer in region-1. Hence, to some extent, the local toughness and failure mode in this interstitial interfacial model will mostly depend on region-2 rather than region-1. In other words, in this case, not a rapid increase in shear strength versus cohesive strength as deduced in [9] but a significant decrease in inter-phase binding strength (refer to table 4) should be responsible for the weakening effect of S-doping.

2.5. Electronic structures of Ni/Ni_3Al interfaces

To thoroughly understand the influence of doped atoms on the properties of the Ni/Ni_3Al interface, electronic structures of the Ni/Ni_3Al interface with or without S-doping are further calculated. Figure 2 illustrates several typical total valence charge density contour plots on the cross section of two coherent interfacial layers of the Ni/Ni_3Al interfacial supercells. Herein, several special sections are selected. That is the cross section with doping inhabitants. For Ni-1 and Ni-2 models, the above-mentioned cross sections are the (4 0 0) and (2 0 0) planes, respectively. For comparison, the total valence charge density contour plots on (2 0 0) and (4 0 0) planes in the S-free model are also presented, as shown in figures 2(*a*) and (*b*).

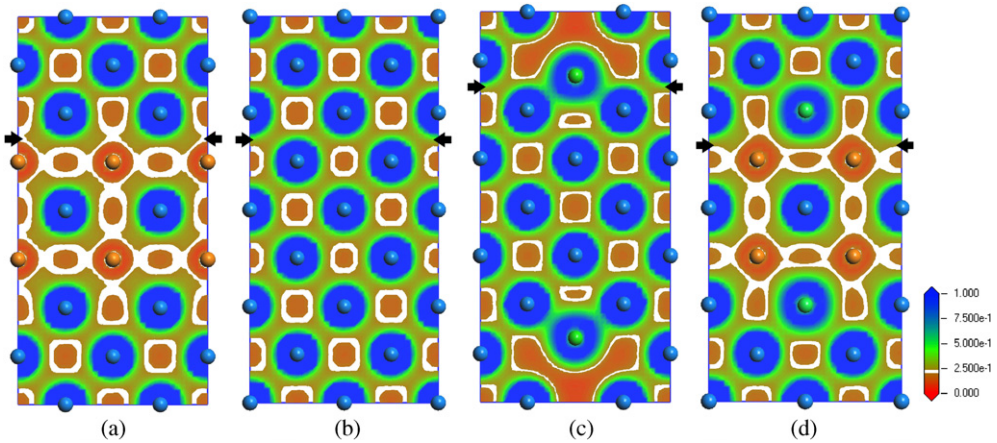

Figure 2. Several typical total valence charge density contour plots on sections across the interface in the Ni/Ni_3Al interface with or without S-doping. (*a*) (2 0 0) plane in the S-free model, (*b*) (4 0 0) plane in the S-free model, (*c*) (4 0 0) plane in the Ni-1 model, (*d*) (2 0 0) plane in the Ni-2 model.

For the clean Ni/Ni_3Al interface, figure 2(*a*) shows that the electronic interaction between FNN Ni–Al atoms in the $\gamma\prime$-Ni_3Al block is stronger than that between FNN Ni–Ni atoms in the γ-Ni block [30]. Moreover, a significant anisotropic build-up of the directional d bonding charge of Ni atoms in the $\gamma\prime$-Ni_3Al block, which is caused mainly by the polarization of p electrons of Al atoms as a result of the p–d hybridization effect [14], along the FNN Ni–Al direction can also be observed. However, for Ni atoms in the γ-Ni block, which is farther from Al in the $\gamma\prime$-Ni_3Al block, the electronic interaction between FNN Ni–Ni atoms displays an obvious isotropy. On the whole, figure 2(*a*) clearly illustrates that the valence charge density in region-2 is rich but poor in region-1. This enrichment and depletion of the valence charge density mean the local electronic interaction in region-2 is stronger than that in region-1, hence a potential inter-phase cleavage fracture in the S-free interface will take place in region-1 between the (0 0 1)$\gamma\prime$ and (0 0 2)$\gamma/\gamma\prime$ layers [9, 10, 12]. Thus, the total valence charge density contour plots for the S-free Ni/Ni_3Al interface provide a direct visual pattern for understanding the inter-phase rupture site indicated in table 4.

With respect to the substitution of Ni by S at the (0 0 2)$\gamma/\gamma\prime$ layer, a similar electron density distribution to the S-free system can also be seen. Figure 2(*d*) shows that the electronic interactions between FNN Ni–Al atoms as well as between FNN Ni–Ni atoms along or across the interface are scarcely changed by S-doping. The only change takes place in region-1, in which the electronic interaction between FNN S–Al atoms displays less anisotropy than that between FNN Ni–Al atoms. Thus the same inter-phase cleavage fracture in region-1 as the S-free interface [10, 12] can also be deduced from figure 2(*d*).

However, different from the S-free and Ni-2 models, the total valence charge density contour plots on the (4 0 0) plane in the Ni-1 model hardly reveal any direct information of inter-phase fracture mode and site. For example, figure 2(*c*) shows the electronic interaction between FNN S–Ni is very strong compared with the Ni-2 model, and this electronic interaction across region-2 is far bigger than that along the (0 0 1)γ atomic layer. According to the elucidation in section 2.1, the substitution of Ni by S at the (0 0 1)γ layer leads to a notable displacement of the doped atoms toward the interface, hence this strong electronic interaction between FNN S–Ni should mainly arise from a larger stress relaxation in the Ni-1 model than in the Ni-2 model (refer to table 1). From this total valence charge density contour plots

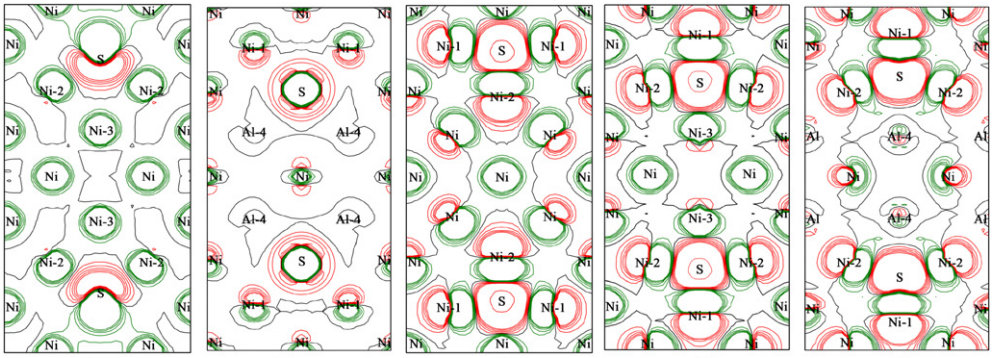

Figure 3. The valence electron density difference on sections across the interface between the S-doped and the S-free Ni/Ni_3Al interfaces, in which red, green and black lines represent increase, decrease and no change in valence electron densities, respectively. (a) (4 0 0) plane in the Ni-1 model, (*b*) (2 0 0) plane in the Ni-2 model, (*c*) (4 0 0) plane in the O-1 model, (*d*) (4 0 0) plane in the O-2 model, (*e*) (2 0 0) plane in the O-3 model.

and the enlarged layer space in region-2 (refer to table 2), it seems to imply the interface would be split along the (0 0 1)γ atomic layer exclusive of the doped atom. However, an exact calculation indicates that the Griffith rupture work W in this situation is 22.5 J m^{-2}, almost 5.5 times as big as 4.138 J m^{-2} deduced from the cleaved surface including S-doping (refer to table 4). Obviously, the cleavage fracture strength in region-2 is far lower than the present shear fracture strength, which means the former will first take place prior to the latter in this doped system. Therefore, for the inter-phase fracture mode and site, not all total valence charge density contour plots on the sections across can yield direct valuable information. In fact, a visual understanding for inter-phase fracture site is also hardly obtained from the total valence charge density contour plots on the (4 0 0) plane in the S-free model (refer to figure 2(*b*)).

In order to further explore why the inter-phase fracture site in the Ni-1 model is changed to region-2 from region-1 in the S-free system, the electron density difference between the S-doped and S-free models is further calculated. Figure 3(*a*) illustrates the variation in charge density on the (4 0 0) plane in the Ni-1 model. As a comparison, several same electron density differences on the (2 0 0) or (4 0 0) plane in other doped systems are also presented in figure 3. From figure 3(*a*), one can see that electron densities at all lattice sites are decreased except for the substituted sites, in which the electron density is added toward Ni-2 at the (0 0 2)$\gamma/\gamma\prime$ layer. This means the electron interaction between FNN atoms in the Ni-1 system is weakened relative to the S-free system. Therefore, a slight decrease in Griffith rupture work W shown in table 4 can be understood in this system. However, a reversion of the inter-phase fracture site from region-1 in the S-free system to region-2 in the present case cannot still be explained. Since doping simultaneously causes lattice relaxation and electronic structure change, for the inter-phase fracture behavior, we think that the influence of elastic strain energies [17] should also be taken into account. It is noted that the layer space in region-2 is significantly larger than that in region-1 even in γ-Ni and $\gamma\prime$-Ni_3Al blocks, and the doped atom is removed far from its previously occupied site (refer to tables 1 and 2). Thus a careful speculation on the existence of large local elastic strain energy in region-2 should be reasonable. Maybe just this high local elastic strain energy leads to the reversion of the inter-phase fracture site in this doped system.

For the Ni-2 system, an evident increase in electron densities around the doped sites and their FNN Ni-1 sites indicates the electron interaction between FNN S–Ni atoms in region-2 is

further enhanced relative to the S-free system. Although the elastic strain energy in region-2 is also larger than that in region-1, it is partially counteracted by its increasing electronic interaction, i.e. atomic bonding energy, hence the Griffith rupture work W drops and the inter-phase cleavage fracture still occurs in region-1, similarly to the S-free system.

In the case of interstitial S-doping, figure 3 shows that most of the extra electrons emerge at the doped sites and the vertexes of doped octahedrons; however, the electron density around vertexes decreases along the doped atoms. For example, in the O-1 model, although Ni-2 at the lower vertex of the doped octahedron gains some extra electrons, they display an obvious directional build-up, i.e. enrichment in region-1 and depletion in region-2. A similar situation can also be seen in other Ni-2 even Ni-3 sub-lattice sites apart from the doped atoms. That means the electronic interaction between FNN Ni–Ni in region-1 increases relative to the S-free system and the atomic bonding energy in region-1 is higher than that in region-2. Undoubtedly, this electron density redistribution should be responsible for the increasing Griffith rupture work W in region-1 shown in table 4, and even for the change of inter-phase cleavage fracture site from region-1 to region-2 to some extent. For O-2 and O-3 systems, one can see that the depletion of electron density in region-2 is slightly more relative to region-1 although an opposite removal of doped atom and its FNN Ni-1 at the $(0\,0\,1)\gamma$ layer results in a stronger electronic interaction between S-doping and its FNN Ni-1 than between S-doping and its FNN Ni-3 or Al-4. Similarly to the Ni-1 model, their separations in region-2 are also far larger than those in region-1 (refer to table 2). Therefore, the inter-phase fracture in region-2 should also be due to the higher local elastic strain energy of region-2 than region-1 in these interstitial doped systems.

3. Conclusion

Using the first-principles plane-wave pseudo-potential method, a systematic investigation of site preference and S-induced embrittlement effect of the Ni/Ni_3Al interface is performed. S-doping either at sub-lattice sites or at octahedral interstitial centers is energetically permissible. Trace element sulfur prefers to substitute for host atoms, especially Ni atoms at the coherent $(0\,0\,2)\gamma/\gamma\prime$ layer as well as at the $(0\,0\,1)\gamma$ layer in the γ-Ni block. S atoms first segregate onto the octahedral interstitial O-2 site bounded by six Ni atoms at the coherent $(0\,0\,2)\gamma/\gamma\prime$ interfacial layer, then O-1 site at the $(0\,0\,1)\gamma$ layer in the γ-Ni block, followed by O-3 site bounded by five Ni and one Al atoms at the coherent $(0\,0\,2)\gamma/\gamma\prime$ layer, and finally O-4 site at the $(0\,0\,1)\gamma\prime$ layer in the $\gamma\prime$-Ni_3Al block. However, all S-doped systems are not as stable as the S-free system. A calculation of Griffith rupture work W shows that S-doping has a deleterious effect on the rupture strength of the Ni/Ni_3Al interface, especially at its preferred substituted and interstitial sites. As a Ni-2 sub-lattice site or O-2 and O-3 interstitial sites at the coherent $(0\,0\,2)\gamma/\gamma\prime$ atomic layer are occupied by S-doping, the rupture strength of S-doped systems decreases by 14.4%, 15.1% and 19.7% compared with the S-free interface, respectively. S-doping not only causes a variation in electronic interactions between FNN atoms in the Ni/Ni_3Al interfacial region, but leads to a significantly relative displacement of doped and host atoms as well as a notable lattice distortion of the Ni/Ni_3Al interfacial supercell. For the substitution of Ni at the coherent $(0\,0\,2)\gamma/\gamma\prime$ layer, the inter-phase cleavage fracture takes place in region-1 between the $(0\,0\,1)\gamma\prime$ layer and the coherent $(0\,0\,2)\gamma/\gamma\prime$ layer as in the S-free interface, while the inter-phase fracture site changes to region-2 between the coherent $(0\,0\,2)\gamma/\gamma\prime$ layer and the $(0\,0\,1)\gamma$ layer and its failure mode would be cleavage via shear in the case of substitution for Ni at the $(0\,0\,1)\gamma$ layer in the γ-Ni block. The segregation of S onto the octahedral interstitial sites at the $(0\,0\,1)\gamma$ layer or the coherent $(0\,0\,2)\gamma/\gamma\prime$ layer is found to be profitable for improvement of the local toughness of the Ni/Ni_3Al interface to a certain

extent, specially at their inter-phase fracture site, i.e. region-2, among which S-doping at the O-1 site is the most favorable. An in-depth analysis on electron structures of the Ni/Ni_3Al interface with or without S-doping reveals that the S-induced embrittlement as well as the change in inter-phase fracture mode and site should be attributed to the mutual influence of atomic bonding energy and local elastic strain energy in the doped systems. As S is doped at the Ni sub-lattice site in the γ-Ni block or O-1 site at the (0 0 1)γ layer as well as O-2 or O-3 sites at the coherent (0 0 2)$\gamma/\gamma\prime$ layer, the large local elastic strain energy in region-2 should be responsible for the reversal of their inter-phase fracture sites.

Acknowledgments

Financial support of this work by the National Natural Science Foundation of China (Nos 50771044, 51071065 and U1037601) and by the Major State Basic Research Development Program of China under grant No 2010CB631206 is gratefully acknowledged.

References

[1] Mitarai Y Y, Ro Y, Maruko T and Harada H 1998 *Metall. Mater. Trans.* A **29** 537–49
[2] Harris K and Wahl J B 2009 *Mater. Sci. Technol.* **25** 147–53
[3] Gheno T, Monceau D, Oquab D and Cadoret Y 2010 *Oxid. Met.* **73** 95–113
[4] Smialek J L 2008 *Mater. Sci. Forum* **595–598** 191–8
[5] Hou P Y and Priimak K 2005 *Oxid. Met.* **63** 113–30
[6] Zhang W, Smith J R, Wang X G and Evans A G 2003 *Phys. Rev.* B **67** 245414
[7] Dong J X, Xie X S and Thompson R G 2000 *Metall. Mater. Trans.* A **31** 2135–44
[8] Liu Y, Chen K Y, Lu G, Zhang J H and Hu Z Q 1997 *Acta Mater.* **45** 1837–49
[9] Chen K, Zhao L R and Tse J S 2003 *Acta Mater.* **51** 1079–86
[10] Peng P, Zhou D W, Liu J S, Yang R and Hu Z Q 2006 *Mater. Sci. Eng.* A **416** 169–75
[11] Chen K, Zhao L R and Tse J S 2004 *Mater. Sci. Eng.* A **365** 80–4
[12] Peng P, Soh A K, Yang R and Hu Z Q 2006 *Comput. Mater. Sci.* **38** 354–61
[13] Gong X F, Yang G X, Fu Y H, Xie Y Q, Zhuang J and Ning X J 2009 *Comput. Mater. Sci.* **47** 320–5
[14] Chen K, Zhao L R and Tse J S 2003 *Phil. Mag.* **83** 1685–98
[15] Chen K, Zhao L R and Tse J S 2003 *Mater. Sci. Eng.* A **360** 197–201
[16] Wu Y X, Li X Y and Wang Y M 2007 *Acta Mater.* **55** 4845–52
[17] Peng P, Jin Z H, Yang R and Hu Z Q 2004 *J. Mater. Sci.* **39** 3957–63
[18] Sanyal S, Waghmare U V, Subramanian P R and Gigliotti M F X 2010 *Scr. Mater.* **63** 391–4
[19] Payne M C, Teter M P, Allan D C, Arias T A and Joannopoulos J D 1992 *Rev. Mod. Phys.* **64** 1045–97
[20] Segall M D, Lindan P J D, Probert M J, Pickard C J, Hasnip P J, Clark S J and Payne M C 2002 *J. Phys.: Condens. Matter* **14** 2717–44
[21] Vanderbilt D 1990 *Phys. Rev.* B **41** 7892–5
[22] Perdew J P, Burke K and Ernzerhof M 1996 *Phys. Rev. Lett.* **77** 3865–8
[23] Francis G P and Payne M C 1990 *J. Phys.: Condens. Matter* **2** 4395–4404
[24] Pulay P 1969 *Mol. Phys.* **17** 197–204
[25] Harada H, Ishida A, Murakami Y, Bhadeshia H K D H and Yamazaki M 1993 *Appl. Surf. Sci.* **67** 299–304
[26] Fischer T H and Almlof J 1992 *J. Phys. Chem.* **96** 9768–74
[27] Sahu B R 1997 *Mater. Sci. Eng.* B **49** 74–8
[28] Hu Q M, Yang R, Xu D S, Hao Y L, Li D and Wu W T 2003 *Phys. Rev.* B **67** 224203
[29] Segall M D, Shah R, Pickard C J and Payne M C 1996 *Phys. Rev.* B **54** 16317–20
[30] Fu C L and Yoo M H 1992 *Mater. Chem. Phys.* **32** 25–36
[31] Eberhart M E, Johnson K H and Latanision R M 1984 *Acta Metall.* **32** 955–9